CeF3-ZnO scintillating nanocomposite for self-lighted photodynamic therapy of cancer

J Mater Sci: Mater Med _####################_
DOI 10.1007/s10856-016-5769-3

Original Research

CeF_3-ZnO scintillating nanocomposite for self-lighted photodynamic therapy of cancer

Tiziano Rimoldi[1] · Davide Orsi[1] · Paola Lagonegro[2] · Benedetta Ghezzi[3] · Carlo Galli[3] · Francesca Rossi[2] · Giancarlo Salviati[2] · Luigi Cristofolini[1]

Received: 15 April 2016 / Accepted: 24 August 2016

Abstract We report on the synthesis and characterization of a composite nanostructure based on the coupling of cerium fluoride (CeF_3) and zinc oxide (ZnO) for applications in self-lighted photodynamic therapy. Self-lighted photodynamic therapy is a novel approach for the treatment of deep cancers by low doses of X-rays. CeF_3 is an efficient scintillator: when illuminated by X-rays it emits UV light by fluorescence at 325 nm. In this work, we simulated this effect by exciting directly CeF_3 fluorescence by UV radiation. ZnO is photo-activated in cascade, to produce reactive oxygen species. This effect was recently demonstrated in a physical mixture of distinct nanoparticles of CeF_3 and ZnO [Radiat. Meas. (2013) 59:139–143]. Oxide surface provides a platform for rational functionalization, e.g., by targeting molecules for specific tumors. Our composite nanostructure is stable in aqueous media with excellent optical coupling between the two components; we characterize its uptake and its good cell viability, with very low intrinsic cytotoxicity in dark.

1 Introduction

Self-Lighting PhotoDynamic Therapy (SLPDT [1]) is a promising innovative cancer therapy that has recently gained interest in the scientific community; it holds the promise to extend to deep cancers the traditional photodynamic therapy (PDT [2]), now commonly applied to treat tumors on the skin or just under it. In usual PDT, a laser light stimulates a photosensitizer (PS) molecule, which promote the production of highly cytotoxic singlet oxygen species ($^1O_2$), causing tissue death through oxidative stress. For this purpose, a broad variety of PS molecules have been considered, i.e., organic dyes and aromatic hydrocarbons, porphyrins, phthalocyanines, and related tetrapyrroles, etc. [3].

From this point of view, SLPDT technique extends the traditional PDT to deep cancer tissues, which cannot be directly reached by light. Recent pilot studies[4, 5] indicate that scintillating nanostructures can potentially be used to activate PDT as a promising deep cancer treatment modality; in this case, scintillator nanostructures play the role of a "local" source of light. When irradiated by X-ray beams as in the traditional radiotherapy of cancer, but at lower doses, they trigger the cascade processes that promote the final production of singlet oxygen[1].

Several classes of nanosystems have been proposed in the literature as effective scintillators for SLPDT, such as nanoparticles, nanotubes, or nanowires [6–9]. Recently, an interdisciplinary collaborating effort proposed an innovative hybrid nanomaterial for X-ray induced PDT [10]. It is based on the stable organic/inorganic interface formed on 3C-SiC@SiO_x core-shell nanowires by functionalization with H_2TPACPP porphyrin. In that case, by the marker kit Singlet Oxygen Sensor Green (SOSG[11]), singlet oxygen generation was demonstrated as a

Electronic supplementary material The online version of this article (doi:10.1007/s10856-016-5769-3) contains supplementary material, which is available to authorized users.

✉ Luigi Cristofolini
luigi.cristofolini@unipr.it

[1] Physics and Earth Science Department, Parma University, Parco Area delle Scienze 7/A, Parma 43124, Italy

[2] IMEM-CNR Institute, Parco Area delle Scienze 37/A, Parma 43124, Italy

[3] Biomedical, Biotechnological and Translational Sciences, Parma University, via Gramsci 14, Parma 43124, Italy

consequence of irradiation with an X-ray beam at 6 MeV. Consequent cell death due to oxidative stress was confirmed by clonogenic survival assay during in vitro experiments.

The lifetime of singlet oxygen in water is about 3–4 μs [12]; it corresponds to a mean free path of about 200 nm for Brownian diffusion. This puts a constraint to the local nature of the treatment: the treatment is effective only if the scintillation mechanism is activated in the target tissue. While being efficient scintillators, nanowires are characterized by low diffusivity. In this respect, nanoparticles could offer advantages since they diffuse easily and, if functionalized with suitable targeting molecules, could target specific tissues or specific tumor cells.

Here we report on the synthesis and the characterization of a novel composite nanostructure, which we deem could be of use for SLPDT. It is based on a nano-CeF_3 as scintillator material, coupled to nano-ZnO, with size in the range 100–500 nm. CeF_3 is known to be an excellent scintillator material where Ce^{3+} ions are the emitters[13, 14]; it has high density (6.16 g/cm), fast response and high radiation resistance[15, 16] in addiction to several advantages provided by the fluoride matrix, such as high quantum yield and high photostability[17]. ZnO has the ability to generate reactive oxygen species (ROS) and to have photocatalytic activity [18, 19]. Moreover the oxide surface offers several functionalization possibilities[20] e.g. with targeting molecules that could be used to drive the nanocomposite to determined cancer tissues, such as folic acid[21], transferrin[22] etc. and with PS molecules, such as porphyrins[10] etc.

As already proven in the literature, a co-precipitated mix of CeF_3 and ZnO nanoparticles shows a strong enhancement of the ZnO luminescence, both using an UV excitation or an X-ray source, due to the FRET optical coupling with CeF_3[23]. In this work, we prepare nanostructures that contain both phases in the same nanocomposite. We detail the synthesis procedure, and we provide morphological and optical characterizations of the nanocomposite; in particular, its UV-excited fluorescence spectrum proves the effective optical coupling between CeF_3 and ZnO. By Energy dispersive X-Ray (EDX) microanalysis, we demonstrate their uptake into human lung adenocarcinoma epithelial cell line (A549), while both by CellTiter-Glo and vital staining with methylene blue assays, we prove the good cytocompatibility of the composite nanostructures. The A549 cell line was chosen because this kind of neoplasia is one of most common yet fatal cancers, often with metastasis diffusing throughout the body. When diagnosed and treated by conventional methods, the 5-year survival rate can be only 17.4 %.

2 Materials and methods

2.1 Chemicals for the NCs synthesis

Cerium nitrate hexahydrate ($Ce(NO_3)_3{\cdot}6H_2O$), ammonium fluoride (NH_4F), sodium hydroxide (NaOH), and polyethylene glycol (PEG-400) are purchased from Sigma Aldrich® S.r.l. Italy, while zinc acetate dihydrate ($Zn(O_2CCH_3)_2{\cdot}H_2O$) is purchased from Carlo Erba Reagents S.r.l. Italy. All reagents are used as received without further purifications.

Deionized (DI) water is produced by a two stage system (Millipore, Elix plus MilliQ) providing a resistivity greater than 18 MΩ·cm with a good stability over several hours.

2.2 Nanostructures characterization

Scanning Electron microscopy (SEM) analyses were performed using a Field-Emission SUPRA40 Zeiss SEM equipped with a GEMINI FESEM detection column and an oxford instruments EDX microanalysis setup.

Transmission electron microscopy (TEM) investigations were performed with a Field-Emission JEOL JEM-2200FS TEM microscope, equipped with High angle annular dark field detector and EDX microanalysis, operated at 200 kV in conventional and Scanning (STEM) mode. For the analysis, the nanostructures were dispersed in ethanol, sonicated and transferred by drop-casting on carbon-coated copper grids.

Raman spectra were acquired using a Jobin-Yvon T64000 triple monochromator spectrometer in subtractive mode, employing 1800 g/mm gratings. Raman light was collected by a confocal microscope in backscattering depolarized geometry with a 50× objective. Excitation at 532 nm was provided by a power controlled DPSS laser, with maximum power to the sample of 1 mW. Typical integration times ranged from 60 to 600 s.

UV-visible absorption spectra in the range 200–900 nm have been measured with a Jasco V550 double-source, double-beam spectrophotometer equipped with a photomultiplier detector (Hamamatsu, R928) in ambient conditions.

Excitation and emission spectra were performed in ambient conditions using a Perkin-Elmer LS50 luminescence spectrometer. Excitation spectra were collected by monitoring the emission at 325 nm and 375 nm using excitation wavelengths between 200–300 nm. Emission spectra were measured exciting at 240 nm and recording the emission between 250 and 450 nm.

2.3 In vitro tests

2.3.1 Cell cultures

Dulbecco's Modified Eagle Medium, fetal bovine serum, antibiotics for cell culture and all reagents were purchased from Gibco Life Technologies (MO, USA); disposable sterile plastics from Costar (Cambridge, MA). A549 human adenocarcinoma alveolar basal epithelial cells were purchased from American Type Culture Collection (ATCC, Manassas, VA, USA) and cultured in DMEM. All media were supplemented with 10 % FBS, penicillin (100 U/ml), streptomycin (100 µg/ml), and L-Glutamine (2 mM), and cells were incubated at 37 °C with 5 % of CO_2 in a water saturated atmosphere.

2.3.2 Direct contact cytotoxicity test

Thirty-thousand cells/ml were seeded onto 96 multiwell plates and allowed to attach. A stock suspension of NCs was freshly prepared. The DMEM in the wells was then replaced with fresh medium containing NCs at increasing concentrations (0, 5, 10, 25, and 50 µg/ml) and the incubation continued at 37 °C and 5 % CO_2 in a humidified atmosphere for 24 and 72 h. Cell viability was analyzed using either a CellTiter-Glo luminescent cell viability assay (Promega, WI, USA), a homogeneous method of determining the number of viable cells based on the quantitation of cellular ATP, or cell counting (data analysis performed by ImageJ software) by optical microscopy (stereomicroscope Nikon SMZ25) after vital staining with Methylene Blue.

2.3.3 Statistical analysis

Data were analyzed using Prism 6 (GraphPad, La Jolla, CA, USA). All values are reported as Mean ± Standard Deviation of six repeated experiments. Differences between group means were evaluated with one-way or multivariate ANOVA statistical tests with Tukey's post hoc tests. No statistically significant (p-values < 0.05) differences were found.

2.3.4 SEM imaging

For SEM observation of A549 cultured for 72 h with the NCs, the samples were first washed with PBS at 37 °C and then fixed using 2.5 % glutaraldehyde in 0.1 M sodium cacodylate buffer for 30' at room temperature. Next the samples were dehydrated with a sequence of treatments in alcohol at increasing concentrations. Finally, the samples were covered with a thin gold layer deposited by sputtering. Cell distribution and morphology were characterized using a Field-Emission SUPRA40 Zeiss SEM equipped with a GEMINI FESEM detection column, operated at 3 keV.

3 Results

3.1 Synthesis procedure

CeF_3-ZnO nanocomposites are synthesized using a two-step wet chemistry synthesis procedure. During the first step, CeF_3 nanoparticles are prepared using a method similar to that reported by Chen[24]. 1 mmol of cerium nitrate hexahydrate ($Ce(NO_3)_3{\cdot}6H_2O$) is dissolved in DI milliQ water. Polyethylene glycol (PEG-400) is added as a surfactant to the $Ce(NO_3)_3{\cdot}6H_2O$ solution; the mixture is left to stir at room temperature for 10 min. Then, a second solution with 3 mmol of ammonium fluoride (NH_4F) in DI milliQ water is added dropwise into the first solution. After stirring for 30 min, the mixture is heated for 2 h at 90 °C. CeF_3 nanoparticles are then collected through centrifugation, washed with DI milliQ water for several times and dried overnight at 45 °C in the oven.

The second step of the synthesis is based on a seed mediated growth: nano-ZnO grows onto the CeF_3 seeds by a method similar to that of Haldar[25]. In our case, 10 mg of CeF_3 seeds are suspended in DI milliQ water, then is added the zinc acetate dihydrate ($Zn(O_2CCH_3)_2{\cdot}H_2O$) and the solution is stirred for a few minutes at 350 rpm at room temperature. At the same time, a sodium hydroxide (NaOH) solution is prepared keeping the stoichiometric ratio of 2 with the zinc precursor. The reaction is triggered adding carefully and dropwise this solution to the CeF_3 seeds suspension. The synthesis is carried out at 50 °C for 1 h while stirring at 350 rpm. The final products are finally washed several times with DI milliQ water before being collected through centrifugation.

3.2 Nanocomposites morphology and elemental analysis

We investigated the morphology of CeF_3 seeds produced by the first step of the synthesis by SEM. Measurements highlight their spherical shape accordingly with previous works present in literature[26, 27]; SEM images and the size distribution are shown in Supplementary Information Figure SI01. The detailed structural and compositional properties of the CeF_3 nanoparticles have been analyzed by TEM; results are reported as Supplementary Information Figure SI02. The High Resolution TEM study shows that the particles are crystalline and the lattice corresponds to hexagonal CeF_3 (JCPDS card 8–45).

The SEM and TEM analysis of the CeF_3-ZnO nanocomposite sample (Fig. 1) reveal conjugate nanostructures with a size in the range 100–500 nm. They form clusters

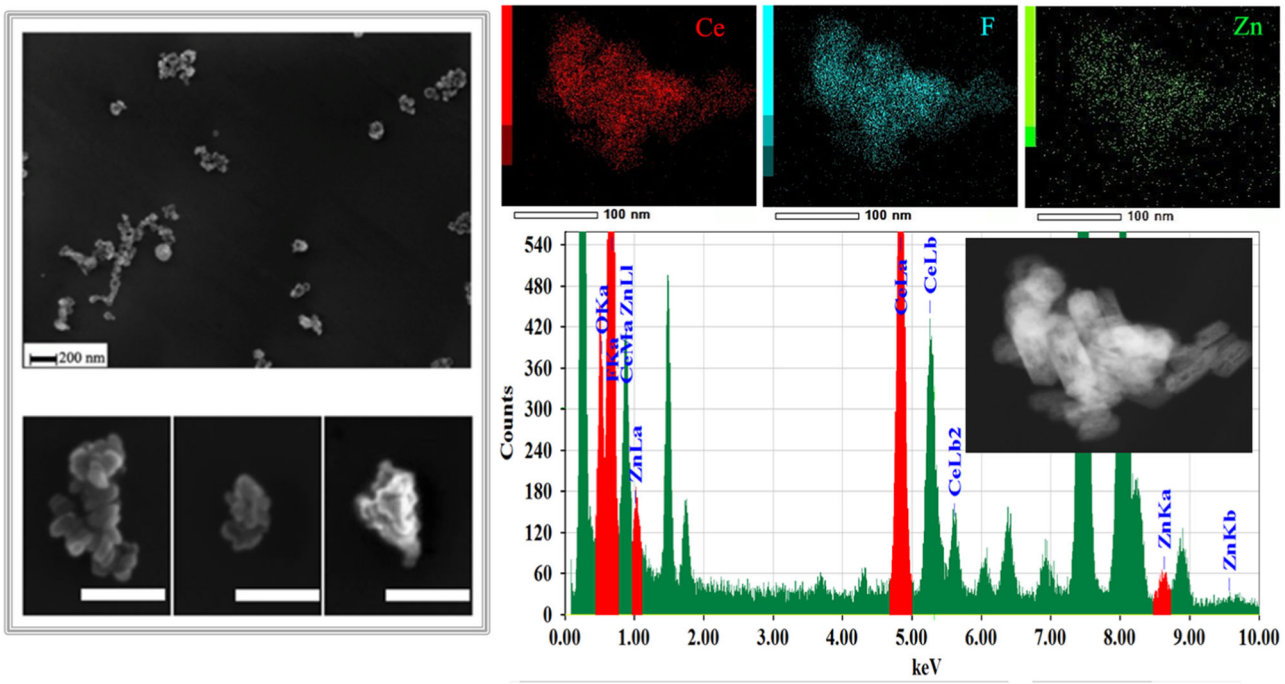

Fig. 1 (*Left*) representative large-area SEM image (*top*) and three magnified details (*bottom*) showing typical CeF_3-ZnO nanocomposites. Scale bars are 200 nm long. (*Right*) STEM-EDX spectrum acquired on an isolated composite and corresponding elemental maps of Cerium (*L edge*), Fluorine (*K edge*), and Zinc (*sum of L and K edges*)

with an irregular pocked surface; a typical SEM image of the ensemble behavior of CeF_3-ZnO nanocomposites suspension dried on flat polished silicon is reported in Fig. 1 (*top left*), together with a detail of single composite nanostructures (*bottom left*).

STEM-EDX spectroscopy and elemental mapping (Fig. 1 right) shows that the conjugates, encompassing several CeF_3 particles, contain Zinc and Oxygen. High Resolution studies (reported as Supplementary Information Figure SI03) confirm that the ZnO domains within the nanostructures are crystalline with standard hexagonal structure (JCPDS card 36–1451), and that the CeF_3 and ZnO lattices are in close contact.

3.3 Raman spectroscopy

The composition of the sample was also investigated using Raman spectroscopy. In Fig. 2, we report the Raman spectrum in the range 250–750 cm^{-1} of the CeF_3 seeds (Panel a), of ZnO reference nanoparticles (Panel b), and of the CeF_3-ZnO nanocomposite (Panel c). We focus our attention on the low-energy peaks corresponding to the lattice vibrations of CeF_3[28] and ZnO[29]: the correspondent Raman bands are shown in Table 1. We find that the spectrum of the nanocomposite is consistently fitted by a linear combination of the spectra from CeF_3 and ZnO (Panel c, black line).

3.4 Nanocomposite optical properties

The luminescence response of the CeF_3-ZnO nanocomposite was compared with that of pristine CeF_3 nanoparticles. Fig. 3 reports the emission spectrum of CeF_3 (red dash line) and ZnO (blue dash-dot line) nanoparticles, as well as for the CeF_3-ZnO nanocomposite (green thick line) generated exciting at $\lambda = 240$ nm, below the band-edge wavelength of ZnO and where CeF_3 has absorbance peaks.

As Supplementary Information, we report with further details the characterization of the excitation and emission spectra at different emission/excitation wavelengths for all the aforementioned samples (figure SI04).

The emission spectra of CeF_3 and ZnO nanoparticles are in agreement with the literature[26, 27, 30, 31]; for nanostructured CeF_3 we find a broad emission peak centered at 325 nm, while for ZnO nanoparticles we observe the near-band-edge emission peak at 365 nm, as well as the broad defect emission band in the visible range of wavelengths. We compare the emission spectrum of the nanocomposite with a linear combination of the spectra of CeF_3 and ZnO nanoparticles. The broad emission peak of CeF_3 in the nanocomposite spectra has 80 % intensity of that of pristine nanostructured CeF_3; 37 % of the lost spectrum area is found as a shoulder at higher wavelength, peaked at 375 nm, e.g., out of the CeF_3 emission peak, as shown in the inset of Fig. 3. The detailed comparison of

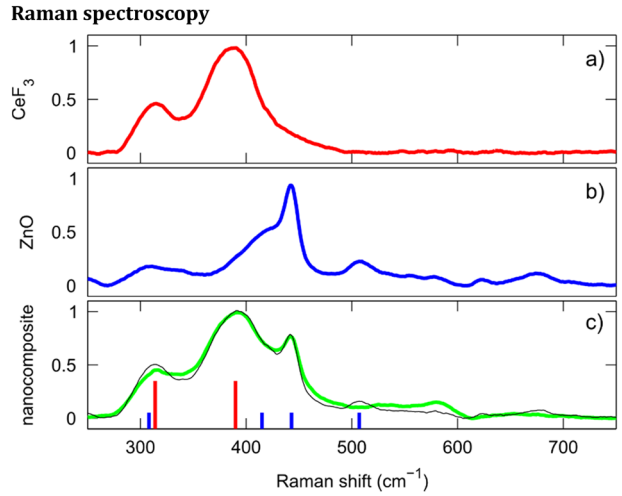

Fig. 2 Normalized Raman spectra of CeF_3 **a** and ZnO **b** nanoparticles and of the CeF_3-ZnO nanocomposites **c**. Panel **c** reports also the linear combination of the spectra of CeF_3 and ZnO nanoparticles (*black line*). The vertical lines (in **c**) are in correspondence of the Raman modes, reported in Table 1, of CeF_3 (*red lines*) and ZnO (*blue lines*), respectively

Table 1 Raman bands of the CeF_3 seed nanoparticles and ZnO reference nanoparticles extracted from spectra in Fig. 2

Wavenumber (cm^{-1})	CeF_3 nanoparticles	ZnO nanoparticles
$\tilde{\nu}_1$		308
$\tilde{\nu}_2$	314	
$\tilde{\nu}_3$	390	
$\tilde{\nu}_4$		415
$\tilde{\nu}_5$		443
$\tilde{\nu}_6$		507

the spectra areas is reported as Supplementary Information Figure SI05.

Finally, a fourfold increase is found in the 200–300 nm region of the excitation spectrum of the nanocomposite with respect to that of pure ZnO (Supplementary Information Figure SI04) measured at emission of 375 nm.

3.5 Cells culture and uptake

Proofs of cellular uptake was obtained via SEM-EDX analysis of A549 cells grown on glass substrate in presence of nanoparticles in the culture medium (10 µg/ml). EDX spectroscopy identifies the presence of Ce and F elements, normally not present in these cells; combined with SEM microscopy, sub-micron clusters of nanostructures internalized by cells can be identified. In Fig. 4a we show a SEM image of a typical A549 cell overlaid with EDX maps of Ce and F (in red) that identifies the localization of the nanostructures. A close inspection at higher magnification (Fig. 4b) shows that brighter aggregates are indeed attached to the outer side of the cell membrane; other clusters of nanostructures -such as the ones marked by red arrows- are clearly surrounded by the cell membrane.

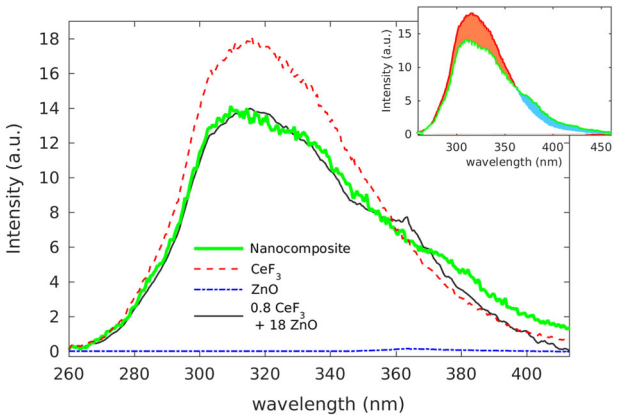

Fig. 3 The luminescence emission of the CeF_3-ZnO nanocomposite excited at 240 nm (*green thick line*), where CeF_3 has its excitation peak, is compared with the analogous emission from pristine CeF_3 (red dash line) and ZnO (blue dash-dot line) nanoparticles, as well as with a linear composition of the two (dark thin line); the differences are discussed in the text. Inset shows the comparison of the spectra of CeF_3 and of the nanocomposite; the area lost on the emission peak of CeF_3 (orange) is partially recovered as a broad shoulder above 360 nm (cyan), indicative of energy transfer to ZnO in the nanocomposite. All spectra are measured on samples of equal weight concentration (0.05 mg/ml) and corrected to account for differences in the instrumental configurations

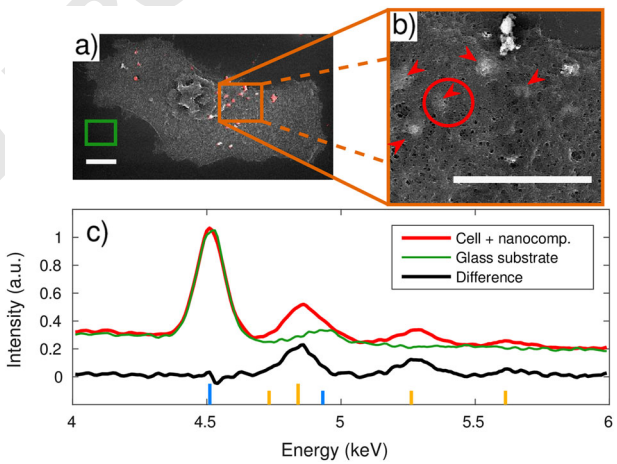

Fig. 4 SEM and EDX spectroscopy performed at 15 keV demonstrate uptake of the nanostructure by the cells. **a** SEM image of an A549 cell cultured in the presence of nanocomposite, overlaid with EDX map of Ce and F elements (*red*). **b** Magnified image shows sub-micron nanostructures inside the cell (*red arrowheads*). *White bars* are 5µm long. **c** EDX spectra of an internalized nanostructure (*red circle* in Panel **b**), compared with that of the glass substrate (*green rectangle* in Panel **a**). Their difference has peaks corresponding to the L lines of Ce (*yellow*), while Ti K lines (*blue*) come only from the substrate

Fig. 4c reports the EDX spectrum collected in correspondence of the region highlighted by the red circle in Fig. 4b (red line); we focus on the 4–6 KeV energy range. We take into account the contribution coming from the glass substrate by subtracting a spectrum measured outside the cell (green line, acquired in the green rectangle in Fig. 4a). The difference curve shows peaks at energies corresponding to the L lines of Cerium (vertical yellow lines in the figure) as a confirmation of the presence of composite nanostructures inside the cell.

3.6 Cytotoxicity evaluation

The cytocompatibility of CeF_3 nanoparticles and CeF_3-ZnO nanocomposites has been evaluated by measuring the viability of A549 cells exposed to increasing concentrations of nanostructures, in the range 0–50 µg/ml, at 24 and 72 hours of culture. Viability has been assessed by CellTiter-Glo assay (Fig. 5) and by counting viable cells marked by methylene blue staining (reported as Supplementary Information, Figure SI07). Both assays shows consistent results; even at the highest concentration, cell proliferation does not decrease in the presence of nanoparticles.

SEM observations (Fig. 6) support this finding: cells appear spread and well attached to the substrate, displaying lamellopodia and filopodia characteristic of good cellular adhesion. Cell membranes possess the typical morphology of healthy living cells both in absence and in presence of nanoparticles, and no morphological changes characteristic of cellular degradation or programmed cell death, such as membrane blebs and rounded apoptotic bodies, were observed. Cytoplasmic protrusions, identifiable as microvilli for size and shape[32], have been identified as the structures of contact between the cell membrane and the nanostructure clusters. The contact, mediated by cellular extension (Fig. 6d), is established with all the tested nanostructures during uptake, as typical of some endocytosis pathways [33, 34].

4 Discussion

Electron microscopy (SEM/TEM/HRTEM, and STEM-EDX spectroscopy) demonstrates that the two-steps synthesis effectively produces nanocomposites with size in the range 100–500 nm, where nanocrystalline domains of CeF_3 and ZnO are in close contact (Fig. 1).

The composition of the nanostructure is confirmed by Raman spectroscopy (Fig. 2). No other chemical species or spurious phases besides CeF_3 and ZnO have been

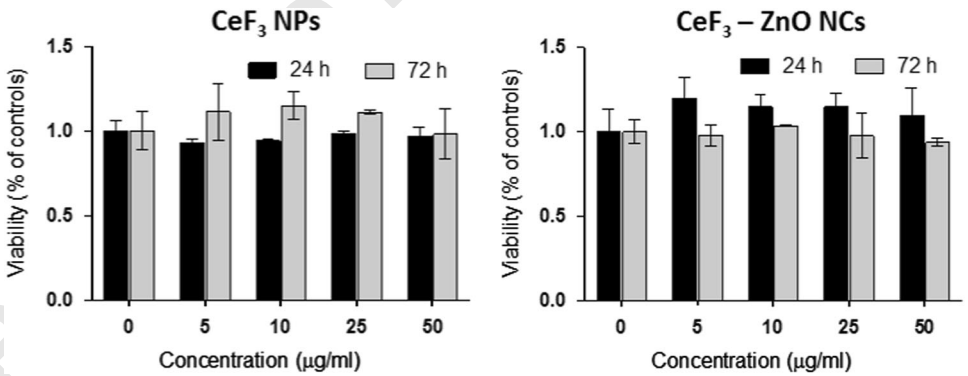

Fig. 5 Viability histograms, evaluated by CellTiter-Glo assay, of A549 cells cultured for 24 and 72 hours in absence or in presence of different concentrations of CeF_3 nanoparticles and CeF_3-Zn0 nanocomposites. No cytotoxicity was observed within 72 hours, in the 0–50 µg/ml concentration range. Statistical analysis does not reveal any significant difference between the groups

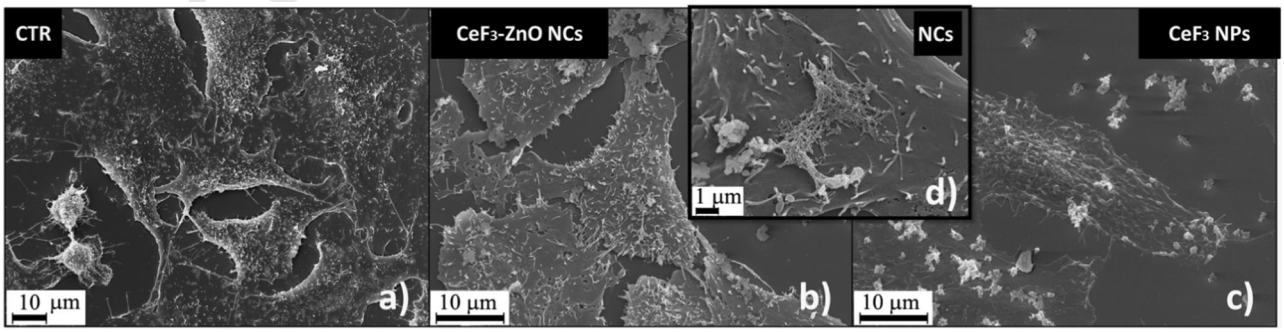

Fig. 6 SEM microphotographs of A549 cells cultured for 72 h with 0 µg/ml (**a**), 50 µg/ml of CeF_3-ZnO NCs (**b**) and 50 µg/ml of CeF_3 NPs (**c**). Detail of a representative A549 cell with CeF_3-ZnO NCs, showing the microvilli assisting cellular uptake (**d**)

synthesized by our approach, at least within the sensitivity of this technique, as they would result in extra peaks in the spectrum. For instance, CeO_2 has a single peak at 464 cm^{-1} in this energy window[35], while ZnF_2 have vibrations at 253, 350 and 522 cm^{-1}. None of these peaks appear in our data[36]. UV-visible absorption spectroscopy provides a complementary evidence that the nanocomposite contains both nanostructured ZnO and CeF_3 (Supplementary Information, Figure SI06). We find the four absorbance peaks of nanostructured CeF_3 below 250 nm, as well as the optical absorption band edge of ZnO at 350 nm.

While these techniques are sensitive to morphology and chemical composition, nothing can be inferred regarding the optical coupling between CeF_3 and ZnO, which is a central point in view of the foreseen application to SLPDT. This issue is addressed by luminescence spectroscopy.

The luminescence spectrum of the nanocomposite (Fig. 3) excited at 240 nm shows that the emission contribution of CeF_3, a broad peak centered at 325 nm, is altered by a shoulder at 375 nm which is compatible with the ZnO near band-edge emission (see Fig. 5 of ref.[37]). We calculate that the emission at 375 nm in the nanocomposite is 18 times stronger than in pristine ZnO nanoparticles excited at 240 nm; this means that when the nanostructure is excited where CeF_3 has maximum absorbance/excitation, ZnO near band-edge emission is excited with efficiency *much higher* than in pristine ZnO nanostructures.

We interpret these results as due to optical coupling between CeF_3 and ZnO. This is rationalized in terms of the energy levels of CeF_3 and ZnO as represented in Fig. 7. A similar scheme was proposed in ref.[23] for a physical mix of nanoparticles, and explained in term of FRET optical coupling. In physical blend of CeF_3 and ZnO nanoparticles, a factor 4 increase in ZnO X-ray luminescence was observed[23]: for our nanostructure, we expect higher enhancement under X-ray irradiation due to the close contact between the two materials at the level of the single composite nanostructure.

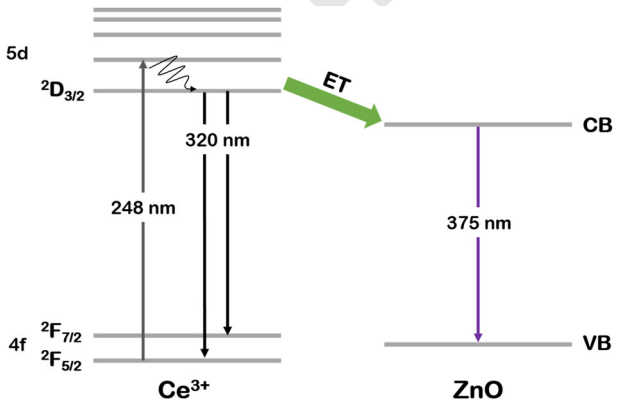

Fig. 7 Scheme of the energy transfer postulated for the CeF_3-ZnO composite nanostructure. Electronic structures are taken from literature both for CeF_3[38] and for ZnO[31]

Moreover, from the position of the ZnO near band-edge emission shoulder (375 nm), basing on the literature [37] reporting the dependence of the ZnO near band-edge emission on the size of nanoparticles, we deduce a typical size of 18–20 nm for ZnO nanocrystals in the nanocomposite. For comparison, a shoulder at 365 nm as found in pristine ZnO nanoparticles corresponds to a size of 5–6 nm.

The use of these nanostructures for SLPDT Therapy requires them to be in contact with cell membranes or be internalized inside cells. Furthermore, they have to be cytocompatible in the absence of light stimuli; upon uptake, nanostructures must not compromise cell viability until singlet oxygen is generated. To test if this happens, we cultured A549 human lung adenocarcinoma epithelial cells with CeF_3-ZnO nanocomposites and we investigated the interactions between them and cells in vitro by CellTiter-Glo assay, by counting viable cells marked by methylene blue staining and by SEM microscopy.

We chose a lung cancer cell line because this kind of neoplasia is one of most common yet fatal cancers, often with metastasis diffusing throughout the body. When diagnosed and treated by conventional methods, the 5-year survival rate can be only 17.4 % ("Surveillance, Epidemiology and End Results Program", National Cancer Institute, Retrieved 15 July 2014).

Using SEM microscopy and EDX spectroscopy, we proved that the nanocomposites are internalized into the cells. Both assays highlight no cytotoxicity on A549 cells within 72 h, in the 0–50 µg/ml concentration range. Statistical analysis of the results of in vitro viability tests does not reveal any significant difference between the nanocomposites and pristine CeF_3 nanoparticles. We conclude that the nanocomposites do not affect neither cellular adhesion nor proliferation, and that they did not elicit any cytotoxic activity.

5 Conclusions

We present a novel composite nanostructure, where we coupled CeF_3 seed nanoparticles to act as scintillators to excite ZnO, a material known to produce ROS. The synthesis of the nanocomposite follows a two-step procedure. In the first step, CeF_3 seed nanoparticles are synthesized in water; in the second step, ZnO nanostructures are grown onto the seed surface, resulting in the formation of nanostructures with size in the range 100–500 nm. In vitro tests with alveolar basal epithelial cells from human adenocarcinoma (A549 cell line) demonstrate that this

proposed SLPDT nanocomposite shows good cellular uptake and has very low cytotoxicity. We characterized the UV-excited luminescence properties of the nanostructure, demonstrating the optical coupling and the energy transfer between its two components. We speculate that ZnO domains in the nanostructure can be excited by the UV emission of CeF_3 also when the nanostructure is irradiated with highly penetrating X-rays from medical facilities.

Within this respect, we believe that this composite nanostructure is of potential interest for the Self-Lighted Photodynamic Therapy.

Compliance with ethical standards

Conflict of interest The authors declare that they have no competing interests.

References

1. Juzenas P, Chen W, Sun Y-P, Coelho MAN, Generalov R, Generalova N, et al. Quantum dots and nanoparticles for photodynamic and radiation therapies of cancer. Adv Drug Deliv Rev. 2008;60:1600–14.
2. Dolmans DEJGJ, Fukumura D, Jain RK. TIMELINE: Photodynamic therapy for cancer. Nat Rev Cancer 2003;3:380–7.
3. Bonnett R. Photosensitizers of the porphyrin and phthalocyanine series for photodynamic therapy. Chem Soc Rev. 1995;24:19
4. Chen W, Zhang J Using nanoparticles to enable simultaneous radiation and photodynamic therapies for cancer treatment. J Nanosci Nanotechnol. 2006;6:1159–66.
5. Liu Y, Chen W, Wang S, Joly AG. Investigation of water-soluble X-ray luminescence nanoparticles for photodynamic activation. Appl Phys Lett. 2008;92:043901.
6. Lal S, Clare SE, Halas NJ Nanoshell-enabled photothermal cancer therapy: impending clinical impact. Acc Chem Res. 2008;41:1842–51.
7. Llusar M, Sanchez C. Inorganic and hybrid nanofibrous materials templated with organogelators. Chem Mater. 2008;20:782–820.
8. Zou X, Yao M, Ma L, Hossu M, Han X, Juzenas P, et al. X-ray-induced nanoparticle-based photodynamic therapy of cancer. Nanomedicine 2014;9:2339–51.
9. Clement S, Deng W, Camilleri E, Wilson BC, Goldys EM. X-ray induced singlet oxygen generation by nanoparticle-photosensitizer conjugates for photodynamic therapy: determination of singlet oxygen quantum yield. Sci Rep. 2016;6:19954.
10. Rossi F, Bedogni E, Bigi F, Rimoldi T, Cristofolini L, Pinelli S, et al. Porphyrin conjugated SiC/SiOx nanowires for X-ray-excited photodynamic therapy. Sci Rep. 2015;5:7606
11. SOSG kit, produced by Molecular Probes and commercialized by Life Technologies, product information: "Singlet Oxyg. Sens. Green Reagent", Revis. 30/01/2004, http://tools.lifetechnologies.com/content/sfs/manuals/mp36002.pdf.
12. Kuimova MK, Yahioglu G, Ogilby PR. Singlet Oxygen in a Cell: Spatially Dependent Lifetimes and Quenching Rate Constants. J Am Chem Soc. 2009;131:332–40.
13. Gai S, Yang P, Li X, Li C, Wang D, Dai Y, et al. Monodisperse CeF_3, CeF_3:Tb^{3+}, and CeF_3:Tb^{3+}@LaF_3 core/shell nanocrystals: synthesis and luminescent properties. J Mater Chem. 2011;21:14610
14. Clement S, Deng W, Drozdowicz-Tomsia K, Liu D, Zachreson C, Goldys EM. Bright, water-soluble CeF3 photo-, cathodo-, and X-ray luminescent nanoparticles. J Nanoparticle Res. 2015;17:7
15. Zhu L, Li Q, Liu X, Li J, Zhang Y, Meng J, et al. Morphological control and luminescent properties of CeF_3 nanocrystals. J Phys Chem. C 2007;111:5898–903.
16. Moses WW, Derenzo SE. Cerium fluoride, a new fast, heavy scintillator. IEEE Trans Nucl Sci. 1989;36:173–6.
17. Jacobsohn LG, Sprinkle KB, Roberts SA, Kucera CJ, James TL, Yukihara EG, et al. Fluoride nanoscintillators. J Nanomater. 2011;2011:1–6.
18. Sakthivel S, Neppolian B, Shankar MV, Arabindoo B, Palanichamy M, Murugesan V. Solar photocatalytic degradation of azo dye: comparison of photocatalytic efficiency of ZnO and TiO_2. Sol Energy Mater Sol Cells. 2003;77:65–82.
19. Villani M, Rimoldi T, Calestani D, Lazzarini L, Chiesi V, Casoli F, et al. Composite multifunctional nanostructures based on ZnO tetrapods and superparamagnetic Fe_3O_4 nanoparticles. Nanotechnology 2013;24:135601.
20. Kolb HC, Sharpless KB. The growing impact of click chemistry on drug discovery. Drug Discov. Today 2003;8:1128–37.
21. Mitra S, S B, Patra P, Chandra S, Debnath N, Das S, et al. Porous ZnO nanorod for targeted delivery of doxorubicin: in vitro and in vivo response for therapeutic applications. J Mater Chem. 2012;22:24145.
22. Pan J, Sun S-K, Wang Y, Fu Y-Y, Zhang X, Zhang Y, et al. Facile preparation of hyaluronic acid and transferrin co-modified Fe_3O_4 nanoparticles with inherent biocompatibility for dual-targeting magnetic resonance imaging of tumors in vivo. Dalt Trans. 2015;44:19836–43.
23. Sahi S, Chen W. Luminescence enhancement in CeF_3/ZnO nanocomposites for radiation detection. Radiat Meas. 2013;59:139–43.
24. Sun Z, Li Y, Zhang X, Yao M, Ma L, Chen W. Luminescence and Energy transfer in water soluble CeF_3 and CeF_3:Tb_3+ nanoparticles. J Nanosci Nanotechnol. 2009;9:6283–91.
25. Haldar KK, Sen T, Patra A. Au@ZnO core-shell nanoparticles are efficient energy acceptors with organic dye donors. J Phys Chem. C 2008;112:11650–6.
26. Kovács M, Valicsek Z, Tóth J, Hajba L, Makó É, Halmos P, et al. Multi-analytical approach of the influence of sulphate ion on the formation of cerium(III) fluoride nanoparticles in precipitation reaction. Colloids Surfaces A Physicochem Eng Asp. 2009;352:56–62.
27. Sun Z, Li Y, Zhang X, Yao M, Ma L, Chen W. Luminescence and energy transfer in water soluble CeF_3 and CeF_3:Tb^{3+} nanoparticles.
J Nanosci Nanotechnol. 2009;9:6283–91.
28. Bauman RP, Porto SPS. Lattice vibrations and structure of rare-earth fluorides. Phys Rev. 1967;161:842–7.
29. Sato-Berrú RY, Vázquez-Olmos A, Fernández-Osorio AL, Sotres-Martínez S. Micro-Raman investigation of transition-metal-doped ZnO nanoparticles. J Raman Spectrosc. 2007;38:1073–6.
30. Wang YS, Thomas PJ, O'Brien P. Nanocrystalline ZnO with Ultraviolet Luminescence. J Phys Chem. B 2006;110:4099–104.
31. Djurišić AB, Leung YH. Optical properties of ZnO nanostructures. Small. 2006;2:944–61.
32. Porter KR, Todaro GJ, Fonte V. A scanning electron microscope study of surface features of viral and spontaneous transformants of mouse BALB/3T3 cells. J Cell Biol. 1973;59:633–42.
33. Conner SD, Schmid SL. Regulated portals of entry into the cell. Nature. 2003;422:37–44.
34. Zhang S, Gao H, Bao G. Physical principles of nanoparticle cellular endocytosis. ACS Nano. 2015;9:8655–71.

35. Popović ZV, Dohčević-Mitrović Z, Cros A, Cantarero A. Raman scattering study of the anharmonic effects in CeO 2− y nanocrystals. J Phys Condens Matter. 2007;19:496209.
36. Porto SPS, Fleury Pa, Damen TC. Raman spectra of TiO_2, MgF_2, ZnF_2, FeF_2, and MnF_2. Phys Rev. 1967;154:522–6.
37. Irimpan L, Nampoori VPN, Radhakrishnan P, Deepthy A, Krishnan B. Size dependent fluorescence spectroscopy of nanocolloids of ZnO. J Appl Phys. 2007;102:063524
38. Riwotzki K, Meyssamy H, Schnablegger H, Kornowski A, Haase M. Liquid-phase synthesis of colloids and redispersible powders of strongly luminescing $LaPO_4$:Ce,Tb nanocrystals. Angew Chemie Int Ed. 2001;40:573–6.

Journal : **10856**
Article : **5769**

Springer
the language of science

Author Query Form

Please ensure you fill out your response to the queries raised below and return this form along with your corrections

Dear Author

During the process of typesetting your article, the following queries have arisen. Please check your typeset proof carefully against the queries listed below and mark the necessary changes either directly on the proof/online grid or in the 'Author's response' area provided below

Queries	Details Required	Author's Response
AQ1	Please provide accessed date in the reference [11].	